Effect of the helicity injection rate and the Lundquist number on spheromak sustainment

Pablo Luis García-Martínez, Leandro Gabriel Lampugnani, and Ricardo Farengo

Citation: Physics of Plasmas (1994-present) **21**, 122511 (2014); doi: 10.1063/1.4903905
View online: http://dx.doi.org/10.1063/1.4903905
View Table of Contents: http://scitation.aip.org/content/aip/journal/pop/21/12?ver=pdfcov
Published by the AIP Publishing

Effect of the helicity injection rate and the Lundquist number on spheromak sustainment

Pablo Luis García-Martínez,[1,a)] Leandro Gabriel Lampugnani,[2] and Ricardo Farengo[2]
[1]*Consejo Nacional de Investigaciones Científicas y Técnicas (CONICET) and Sede Andina—Universidad Nacional de Río Negro (UNRN), Av. Bustillo 9500, 8400 San Carlos de Bariloche, Río Negro, Argentina*
[2]*Instituto Balseiro and Centro Atómico Bariloche (CAB-CNEA), Av. Bustillo 9500, 8400 San Carlos de Bariloche, Río Negro, Argentina*

(Received 6 October 2014; accepted 26 November 2014; published online 11 December 2014)

The dynamics of the magnetic relaxation process during the sustainment of spheromak configurations at different helicity injection rates is studied. The three-dimensional activity is recovered using time-dependent resistive magnetohydrodynamic simulations. A cylindrical flux conserver with concentric electrodes is used to model configurations driven by a magnetized coaxial gun. Magnetic helicity is injected by tangential boundary flows. Different regimes of sustainment are identified and characterized in terms of the safety factor profile. The spatial and temporal behavior of fluctuations is described. The dynamo action is shown to be in close agreement with existing experimental data. These results are relevant to the design and operation of helicity injected devices, as well as to basic understanding of the plasma relaxation mechanism in quasi-steady state. © *2014 AIP Publishing LLC*. [http://dx.doi.org/10.1063/1.4903905]

I. INTRODUCTION

The spheromak is a toroidal magnetic equilibrium spontaneously formed inside a simply connected chamber (or flux conserver) as a result of a magnetic relaxation process.[1] This equilibrium is well described by the force-free state $\nabla \times \mathbf{B} = \lambda_n \mathbf{B}$, with boundary condition $\mathbf{B} \cdot \mathbf{n} = 0$ (note that this is an eigenvalue problem with non-trivial solutions for a set of discrete eigenvalues λ_n). As a result of magnetic relaxation, the local quantity $\lambda \equiv \mu_0 J_{||}/B$ becomes spatially uniform and approaches the first eigenvalue λ_1. The explanation for this behavior is given by relaxation theory:[2] localized magnetic reconnection events are able to rapidly dissipate magnetic energy, while leaving total magnetic helicity almost unaffected. This argument can be used to explain not only the formation but also the sustainment of spheromak configurations. The key is to realize that helicity is conserved on a time scale long compared to the Alfvén and reconnection times, and only decays on the resistive diffusion time scale. This implies that the spheromak configuration can be sustained by the injection of magnetic helicity at the appropriate rate. A steady (or quasi-steady) state can then be reached when the helicity injection rate is equal to the helicity dissipation rate.

A common method to inject helicity into the system is to connect the flux conserver to a magnetized coaxial gun.[3] It consists of a pair of electrodes that intercept magnetic flux and some means to produce a voltage difference across this flux. In experiments, this is typically achieved using a capacitor bank.[4,5] An alternative approach has been recently proposed, where an electric field perpendicular to the external magnetic flux is generated by tangential boundary flows.[6] An advantage of this approach is that it can be correctly described by the magnetohydrodynamic (MHD) model. Furthermore, the feasibility of forming and sustaining spheromak configurations has been already demonstrated. This helicity injection mechanism can be interpreted as produced by the motion of the footpoints of the penetrating (open) magnetic field,[7] which has been proposed to be the dominant process in the solar corona.[8]

When helicity is injected using a coaxial gun, either by an electrostatic potential difference or by tangential boundary flows, the corresponding boundary conditions are axisymmetric. The relaxed state towards which the plasma evolves is also axisymmetric. However, Cowling's antidynamo theorem[9] assures us that a steady axisymmetric MHD sustainment process is not possible. Accordingly, magnetic fluctuations are always observed during spheromak sustainment.[3,5,10,11] Various magnetic dynamo mechanisms were identified by measurements in the Spheromak Experiment (SPHEX)[12] that rely on time-varying MHD fluctuations. Despite the fundamental role of fluctuations on spheromak sustainment, there is no closed theory to describe their behavior. A better understanding would be valuable for practical purposes (e.g., to improve the design of confinement devices relying on helicity injection) as well as relevant to basic research on magnetic relaxation and plasma self-organization.

Previous efforts to model the formation and sustainment of electrostatically driven spheromaks using an artificial, high resistivity layer to impose a voltage difference across the electrodes were able to reproduce and study some important features of the relaxation process, such as the dominance of the toroidal $n = 1$ mode and the saturation of the modes to a fixed amplitude.[13–15] However, other ubiquitous phenomena such as the spontaneous rotation of the central flux column[16–18] or the evolution of the mean magnetic configuration close to the kink stability threshold described by a linear λ profile[10,19] were not reproduced.

The main objective of this work is to improve the current understanding of the dynamics of magnetic relaxation

a)Electronic address: pablogm@cab.cnea.gov.ar

inside a simply connected flux conserver during sustainment via helicity injection. To that end, a pair of concentric electrodes is used to introduce magnetic flux and tangential boundary flows are applied to inject magnetic helicity. In contrast with previous works, in this study, the helicity injection rate (given by the intensity of the boundary flows) and the helicity dissipation rate (controlled by the Lundquist number) are varied simultaneously to maintain a quasi-steady state configuration representative of real spheromaks driven by coaxial plasma guns. This enabled us to identify and characterize in a systematic way, the different regimes of sustainment that arises as the intensity of the magnetic helicity influx to the system is varied. The novel results include: (1) verification of the relaxation behavior in a wide range of helicity injection rates and identification of the minimum Lundquist number required for this dynamics, (2) description of the behavior of the q profile in the different regimes of sustainment, (3) estimation of the scaling of the magnetic fluctuations amplitude with the Lundquist number, and (4) an improved description of the flow fields and dynamo electric fields during sustainment.

As described in Sec. II A, the imposed tangential boundary flows produce a net radial electric field at the electrodes, acting as a source of toroidal magnetic flux. In this sense, the helicity injection mechanism used here may be regarded as an alternative approach to model electrostatically driven spheromaks. In fact, several aspects of the sustainment observed in experiments could be reproduced and studied for the first time. In particular, the distortion of the central flux column, its frequency of rotation and the behavior of the λ profile for different helicity injections rates are analyzed. Also, the presence of a single mode dynamo in the central region and a different dynamo process near the magnetic axis is observed and shown to be in close agreement with the published experimental data.[12]

The rest of the paper is organized as follows. The model, including the numerical method, the geometry, the boundary conditions and the initial condition, as well as the strategy to set the helicity balance are described in Sec. II. The results are presented in Sec. III and the conclusions are summarized in Sec. IV.

II. MODEL DESCRIPTION

The plasma is modeled using the visco-resistive MHD equations in the zero β approximation. The evolution equations for $\mathbf{u}$ and $\mathbf{B}$ are

$$\partial_t \mathbf{u} + \mathbf{u}\cdot\nabla\mathbf{u} = (\mathbf{J}\times\mathbf{B})/\rho_0 + \nu\nabla\cdot\Pi, \tag{1}$$

$$\partial_t \mathbf{B} + \nabla\times\mathbf{E} = 0, \tag{2}$$

where $\mathbf{J}=\nabla\times\mathbf{B}$, $\mathbf{E}=-\mathbf{u}\times\mathbf{B}+\eta\mathbf{J}$, and $\Pi=(\nabla\mathbf{u}+\nabla\mathbf{u}^T) - (2/3)\times(\nabla\cdot\mathbf{u})$, ρ_0 is the uniform plasma density, ν is the kinematic viscosity, and η is the resistivity. These equations are normalized with the chamber radius a, the externally imposed magnetic flux ψ_0, and the Alfvén speed c_A. In addition, $\mathbf{B}$ and $\mathbf{J}$ are rescaled with $\sqrt{\mu_0}$ so the constant μ_0 is omitted. The resulting system is solved using standard finite volume techniques,[20] which are already implemented in several freely available codes. Here, the Versatile Advection Code[21,22] is used with a Roe-type solver for the linearized Riemann problem for the MHD equations.[23,24] The divergence free condition of the magnetic field is maintained using the projection method.[22] Validation of the scheme and convergence studies for spheromak conditions has already been presented.[6,25,26]

In the following, time is normalized with the Alfvén time $\tau_A = a/c_A$. The Lundquist number $S=\tau_r/\tau_A$ gives the ratio between the typical resistive time and the Alfvén time. For the resistive time scale, we adopt the definition of Izzo and Jarboe:[27] $\tau_r = 1/(\eta\lambda_1^2)$, where λ_1 is the eigenvalue of the relaxed state. In our geometry, a cylinder with $a=h=1$, $\lambda_1 = 4.955$.[28]

A. Geometry and boundary conditions

The domain is a cylinder of elongation $h/a=1$, with perfectly conducting wall conditions ($\mathbf{B}\cdot\mathbf{n}=0$ and $\mathbf{J}\times\mathbf{n}=0$) and vanishing velocity ($\mathbf{u}=0$) at the cylindrical boundary ($r=a$) and the top end ($z=h$). This is shown in Fig. 1(a). The usual cylindrical coordinate system is used. At the bottom end, two concentric electrodes are simulated by imposing the poloidal flux (i.e., the normal component of the magnetic field) and a tangential flow. The imposed poloidal flux is $\psi(r,z=0)=\psi_0\,\mathcal{C}(r/a)^2(1-r/a)^3$, where $\mathcal{C}=28.935$ is a normalization constant and ψ_0 is the maximum flux imposed by the gun [Fig. 1(b)]. This geometry has already been used to model the SPHEX.[29] If $\mathbf{u}=0$ was imposed at $z=0$, the full set of boundary conditions would lead to vanishing helicity and energy fluxes across the boundary.

Imposing tangential flows at a boundary intercepted by magnetic flux may result in the injection of helicity, as can be inferred from the equation

$$\frac{dH}{dt} = -2\int_V \eta\mathbf{J}\cdot\mathbf{B}\,dV - 2\oint_{\partial V}\left[(\mathbf{A}\cdot\mathbf{B})(\mathbf{u}\cdot\mathbf{n}) - (\mathbf{A}\cdot\mathbf{u})(\mathbf{B}\cdot\mathbf{n})\right]dS, \tag{3}$$

where electrostatic fields as well as resistivity (which causes field line slippage) have been neglected. In Eq. (3), H stands for the relative helicity defined as Finn and Antonsen,[30] and $\mathbf{n}$ denotes the outward directed normal. The last term on the right gives the helicity injection produced by motions of the footpoints of the penetrating (open) magnetic field.[31] Boundary shearing of magnetic fields has been applied to study reconnection events in low-β plasmas relevant to the solar corona.[32]

The computations presented in this work have $u_r=u_z=0$ and $u_\phi = U_0\max[0, 25(2/5-r)r]$, at $z=0$ [Fig. 1(c)]. This flow produces helicity injection across the bottom end of the cylinder because $A_\phi = \psi/(2\pi r)\neq 0$ there. Note that these boundary conditions produce a radial electric field ($E_r = -u_\phi B_z$) at the central electrode that acts as a source of toroidal magnetic flux.

B. Initial condition

The initial condition is a two-dimensional force-free spheromak equilibrium that satisfies

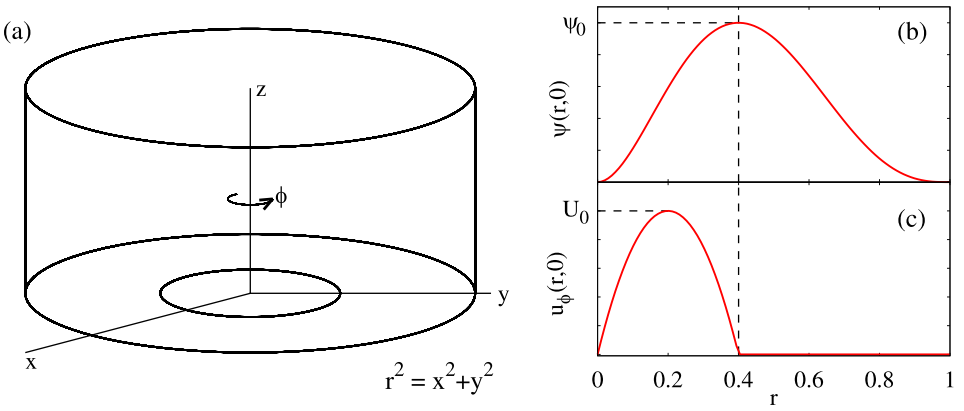

FIG. 1. (a) The domain is a circular cylinder of elongation $h/a = 1$. Cylindrical coordinates are used. (b) Poloidal flux and (c) boundary flow imposed at $z = 0$.

$$\nabla \times \mathbf{B} = \lambda(\psi)\mathbf{B} \tag{4}$$

with $\lambda(\psi) = \bar{\lambda}[1 + \alpha(2\psi - 1)]$. The resulting non-linear Grad-Shafranov equation is solved for the boundary conditions described above. The sign of the slope, α, specifies whether the spheromak is in the sustainment (negative) or decaying (positive) phase.

In this work, we focus on the dynamics of the configuration during the sustainment phase. Consequently, all the simulations start from the solution to Eq. (4) obtained for $\alpha = -0.4$, which corresponds to a marginally unstable equilibrium that models the spheromak configuration during sustainment better than the uniform λ Taylor state.[10,19] The value of $\bar{\lambda}$ is adjusted to produce an adequate poloidal flux value at the magnetic axis ψ_a, which equals the flux amplification factor with the chosen normalization. We take $\bar{\lambda} = 5$, which gives $\psi_a \approx 5.9$.

The resulting configuration is shown in Fig. 2. A colormap of λ along the poloidal plane as well as the flux contours are shown in Fig. 2(a). The thick black line shows the limit between open (those that intercept the boundary) and closed flux surfaces. The $q = 1$ flux surface is shown in red (where q is the safety factor). Fig. 2(b) shows the λ and q profiles. Note that ψ is set to zero at $r = 0$ and at the boundary (excepting at $z = 0$), thus ψ increases as we approach the magnetic axis (where $\psi = \psi_a$).

C. Helicity balance

The set up just described evolves under the action of two competing processes, namely: helicity injection by tangential boundary flows ($\dot{H}_{inj}$) versus resistive dissipation ($\dot{H}_{dis}$). After a transient phase, the system reaches a quasi-steady state, where helicity injection balances dissipation. Our aim is to study this steady state (i.e., sustainment phase) at different helicity injection rates, while maintaining the magnetic helicity content approximately constant. The strategy to accomplish this is described below.

The dominant helicity injection mechanism is provided by the boundary flows imposed at the electrode and can be quantified from the third term on the right of Eq. (3) as $\dot{H}_{inj} = 2\int_0^1 u_\phi A_\phi B_z \, 2\pi r dr$, for the geometry described in Sec. II A. Note that $\dot{H}_{inj} \propto U_0$, so we can use U_0 to control (linearly) the helicity injection rate.

The resistive dissipation is given by the first term on the right of Eq. (3), which is proportional to the resistivity, i.e.,

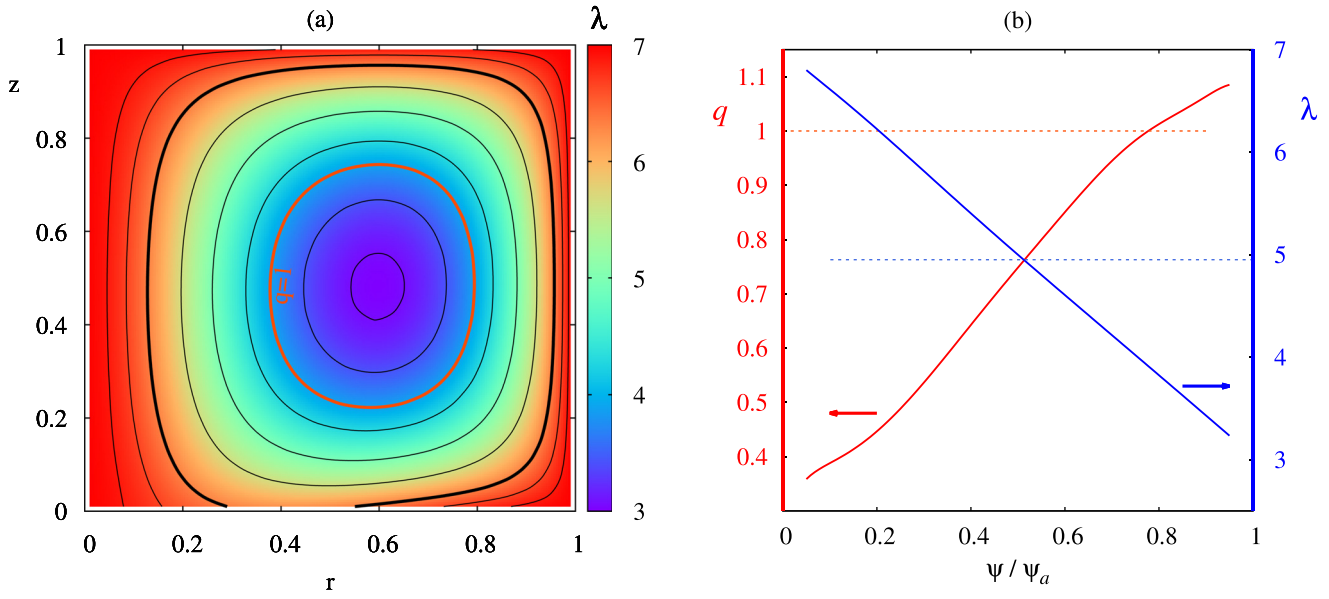

FIG. 2. Initial condition: (a) poloidal flux contours and colormap of λ and (b) profiles of λ and safety factor. This marginally unstable equilibrium models the mean spheromak configuration during the sustainment phase.[10]

$\dot{H}_{dis} \propto \eta$. Since $\mathbf{J} \approx \lambda_1 \mathbf{B}$ in sustainment regime, helicity dissipation is also proportional to the magnetic energy content of the configuration. It should be clear that the latter relationship, which could have also been established for the total helicity content, is only approximate due to the presence of λ gradients and MHD fluctuations.

In the quasi-steady state, the time averaged balance $\dot{H}_{inj} = \dot{H}_{dis}$ holds. An increase in U_0 leads to higher $\dot{H}_{inj}$, which must be balanced by an increment of $\dot{H}_{dis}$ to reach a steady state. If η is held constant, the magnetic energy content will adjust to match this balance. Note that the relation is linear: doubling U_0 doubles the mean magnetic energy in steady state (up to deviations due to gradients and fluctuations). If, on the other hand, the ratio U_0/η is held constant, the mean magnetic energy (and helicity) content in the steady state should be roughly the same at different helicity injection rates.

The simulations presented in this work were obtained for $U_0/\eta = 2000$, which can be expressed in terms of the Lundquist number as $U_0 \approx 80/S$, since $\lambda_1 \approx 5$ in our geometry. As shown in Sec. III, this value approximately maintains the energy and helicity contents of the initial condition employed. The explored range of S extends from 100 (where resistivity does not allow for spheromak sustainment, as will be discussed) to 4000, which is the highest reliable value for the grid resolution used ($100 \times 100 \times 50$). Note that $S = 4000$ in our scaling corresponds to a Lundquist number as high as 10^5 if the standard definition of the resistive length scale (a instead of $1/\lambda_1$) is used.

III. RESULTS AND DISCUSSION

Under the action of the tangential boundary flows the configuration becomes kink unstable, triggering the relaxation process. Fig. 3(a) shows the evolution of ψ_a for three cases with different Lundquist numbers. An initial resistive decay is followed by a poloidal flux amplification event. Since the imposed boundary conditions only induce toroidal magnetic flux, this is a clear signature of the flux conversion

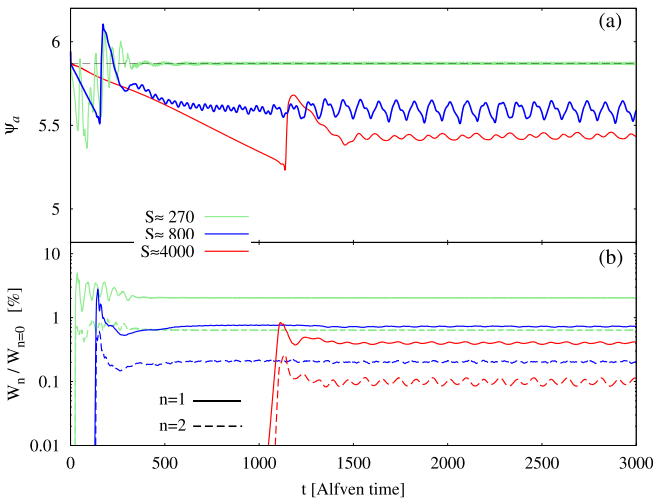

FIG. 3. (a) Evolution of the poloidal flux at the magnetic axis and (b) the magnetic energy content of the first two toroidal modes (relative to the $n = 0$ magnetic energy) for three cases.

mechanism associated to magnetic relaxation. It is well known that such a process necessarily involves non-axisymmetric activity. In agreement, Fig. 3(b) shows that each flux amplification event is preceded by the rapid growth of $n > 0$ modes, where n is the toroidal wave number. The mode's amplitude saturates and, after a transient phase, a quasi-steady state is reached. As expected, the saturation amplitude of the modes decreases with S.

The axisymmetric part of the magnetic configuration (i.e., the $n = 0$ mode) during the quasi-steady state is shown in Fig. 4, for different values of S. Several radial profiles at $z = 0.5$ in the time interval $2000 \le t \le 3000$ are plotted for each case. The oscillations of the $n = 0$ mode are small and the curves almost coincide. See, for instance, the poloidal field profile near the magnetic axis for the case $S = 800$. The profile is thicker in that region due to the temporal oscillations of the mode. This oscillation is connected to the ripple observed in the green curve of Fig. 3(a).

The dashed lines in Fig. 4 show the initial profiles. The magnetic configurations formed after the unstable transient phase are very similar to the initial configuration for a wide range of S. We recall that lower Lundquist numbers involve higher helicity dissipation rates that are balanced by higher helicity injection rates, according to the strategy explained in Sec. II C. This enables us to study the dynamics of magnetic relaxation during sustainment at different helicity injection-dissipation rates, while keeping almost the same mean magnetic configuration.

A. Magnetic energy and helicity during sustainment

Fig. 4 shows that the initial condition can be approximately maintained in steady state for different helicity injection rates. However, small deviations of the final $n = 0$ mode obtained can be observed for different values of S. Moreover, Fig. 4(d) shows that the initial configuration cannot be sustained when resistivity is too high, suggesting the existence of a threshold in the Lundquist number for spheromak sustainment.

To find this threshold and to study the global behavior of the resulting $n = 0$ mode at different helicity injection rates, we computed the magnetic energy ($W_{n=0}$) and magnetic helicity ($H_{n=0}$) during the quasi-steady state phase ($2000 \le t \le 3000$) as a function of S. The results are plotted in Figs. 5(a) and 5(b). The mean value is shown in black (line and points) while the minimum and maximum values during the quoted time interval are shown in orange (line). These quantities are normalized to the initial values. For $S > 150$, a negligible dispersion is observed, i.e., the magnetic energy and helicity of the $n = 0$ mode remain approximately constant in time during sustainment (for each S value).

Note that the profiles shown in Figs. 4(a)–4(c) have smaller field amplitudes for higher S values. This trend is verified, for $S > 200$, in Fig. 5. As pointed out in Sec. II C, the strategy of keeping the ratio U_0/η constant to maintain the helicity content in the steady state is only approximate. However, the deviation in the helicity content is less than 15% for the whole range of S explored. The deviation is due

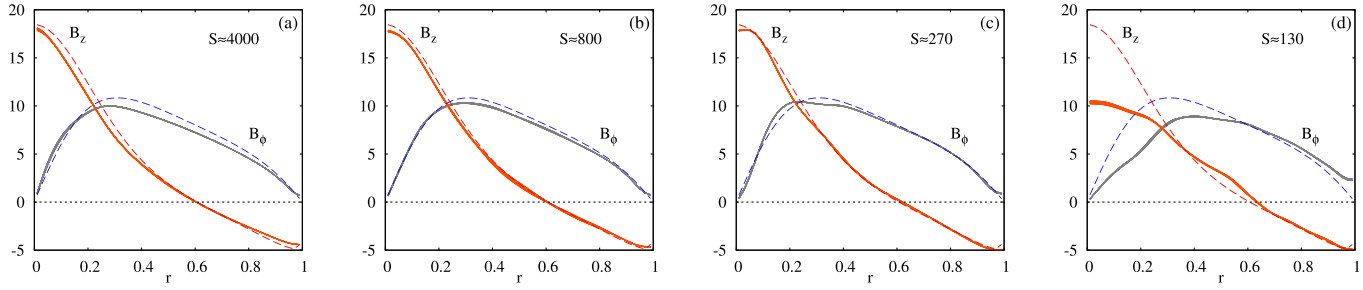

FIG. 4. Poloidal (B_z) and toroidal (B_ϕ) radial profiles at $z=0.5$ of the $n=0$ component. Fifty instantaneous profiles in the time interval $2000 \le t \le 3000$ are plotted (full lines). The dashed lines show the initial profiles.

to sources not included in Eq. (3). Among them, the dominant is the helicity injected by the electrostatic potential established between the electrodes by the $\eta\mathbf{J}$ term. This effect was used as the only source of helicity injection to study spheromak formation and sustainment by other authors.[13]

Theoretical relaxed states have uniform λ equal to the lowest eigenvalue λ_1. Furthermore, it is easy to show that $\lambda_1 = 2W/H$ for those states. Despite the presence of fluctuations and λ gradients in our simulations, we may still compute the average value $\langle\lambda\rangle = 2W_{n=0}/H_{n=0}$, to assess the relaxation behavior in terms of the minimization of magnetic energy relative to magnetic helicity. The results, plotted in Fig. 5(c), show that $\langle\lambda\rangle$ remains remarkably close to the theoretical value λ_1, provided S is large enough. For $S<150$, the value of $\langle\lambda\rangle$ grows indicating that magnetic relaxation cannot operate in this regime. We conclude that $S=150$ is the minimum Lundquist value required for spheromak sustainment in the present set up.

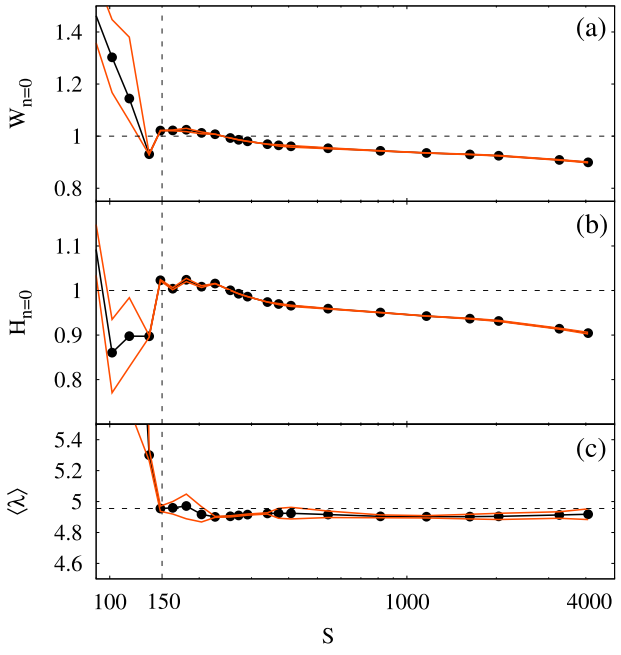

FIG. 5. (a) Magnetic energy, (b) relative magnetic helicity of the $n=0$ mode, and (c) $\langle\lambda\rangle = 2W_{n=0}/H_{n=0}$ during steady state. The energy and helicity are normalized to their initial values. Average values, during the sustainment phase, are shown with black lines and points, while the maximum and minimum values are shown with orange lines.

B. Sustainment regimes

The evolution of ψ_a is different for each of the three cases considered in Fig. 3(a). The behavior of ψ_a as a function of the Lundquist number is shown in Fig. 6(a). The maximum and minimum values of ψ_a during the sustainment phase are shown in orange and the average is shown in black. Different regimes of operation may be identified according to the dispersion of ψ_a (i.e., the amplitude of the temporal oscillation) and the value of the safety factor at the magnetic axis (q_a), as shown in Fig. 6(b). For the analysis of the behavior of the configuration on each regime let us also consider the q and λ profiles. In Fig. 7, these profiles are shown for nine cases spanning the whole range of S values under consideration. Fifty instantaneous profiles during the sustainment phase are plotted for each case (solid lines). The initial profiles are shown with dashed lines.

At high Lundquist numbers [regime (i) in Fig. 6], the magnetic structure has very low magnetic shear ($\propto \partial q/\partial\psi$) and $q\sim 1$ around the magnetic axis. This is clearly seen in Fig. 7(a). This low-shear resonant (since $q\sim 1$) region is

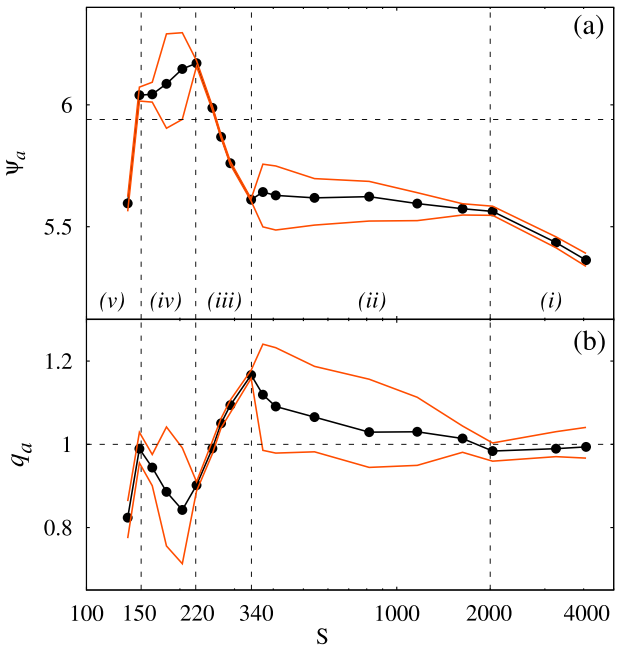

FIG. 6. Poloidal flux (a) and safety factor (b) at the magnetic axis during the sustainment phase. Maximum and minimum values are in orange and the average is in black.

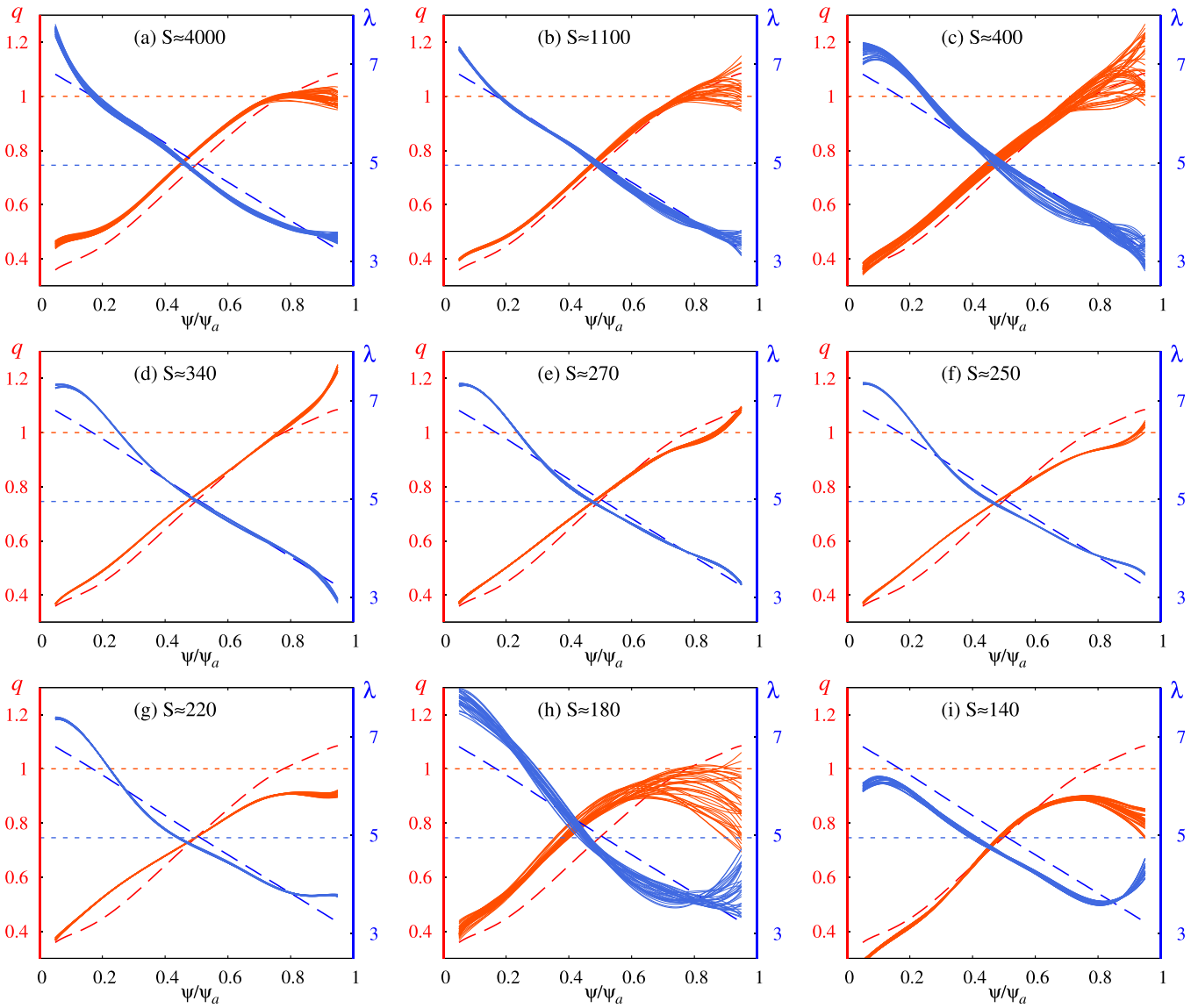

FIG. 7. q and λ profiles during sustainment. Fifty instantaneous profiles during the sustainment phase are shown for each variable. The initial profiles are shown with dashed lines.

slightly larger than the initial $q > 1$ region (see also Fig. 2). The temporal fluctuations of q_a are relatively small but noticeable. At moderate Lundquist numbers [see regime (ii) in Fig. 6 and profiles in Figs. 7(b) and 7(c)], the fluctuations in q_a and ψ_a grow significantly as S decreases. This causes the mean (in time) value of q_a to grow as well. However, the minimum value of q_a remains below unity. Since the initial $q = 1$ surface approximately remains at its original position, this oscillation produces the episodic formation and disappearance of a second resonant $q = 1$ surface and a region of reversed shear.

As S is lowered [regime (iii) in Fig. 6], a drastic change takes place around $S \approx 340$. The oscillations of the underlying $n = 0$ configuration virtually disappear and a region of high magnetic shear develops near the magnetic axis [Fig. 7(d)]. After this, the initial $q = 1$ surface moves towards the magnetic axis [Figs. 7(e) and 7(f)] until it disappears, leaving a zero-shear region around the magnetic axis [Fig. 7(g)]. In the last regime of sustainment, (iv), the oscillations of the $n = 0$ mode reappear giving rise to the sporadic formation of a resonant surface around the magnetic axis [Fig. 7(h)]. However, the mean q-profile in this regime has reversed shear in the central region and q_a remains well below unity. Finally, when the spheromak sustainment threshold is crossed (v) the oscillations of the profiles diminish, the mean λ profile decreases significantly [Fig. 7(i)] and the configuration departs from the minimum energy state.

The overall behavior observed in Figs. 6 and 7 for $S \gtrsim 250$ is in agreement with observations in spheromaks driven by coaxial plasma guns,[10,19] namely, the configuration remains remarkably close to the marginally unstable equilibrium with a linear $\lambda(\psi)$ profile for a wide range of values of S. Note that λ in the open flux region ($\psi/\psi_a \lesssim 0.2$) tends to be larger than that of the initial condition, and smaller in the closed flux region (except for $S = 340$). However, a $\tanh \lambda(\psi)$ profile does not seem to provide a better approximation than the simpler linear profile, specially at high Lundquist numbers. Experimental efforts led to the same conclusion.[19]

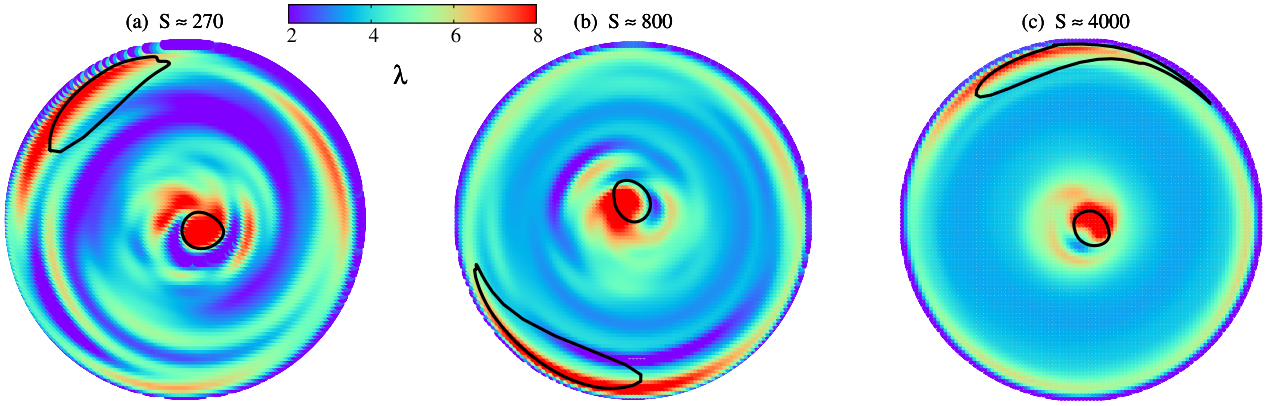

FIG. 8. Instantaneous λ values along the toroidal plane at $z = 0.5$ during sustainment, for different Lundquist numbers representative of the first three regimes of sustainment of Fig. 6. Black lines show the central and return open flux column.

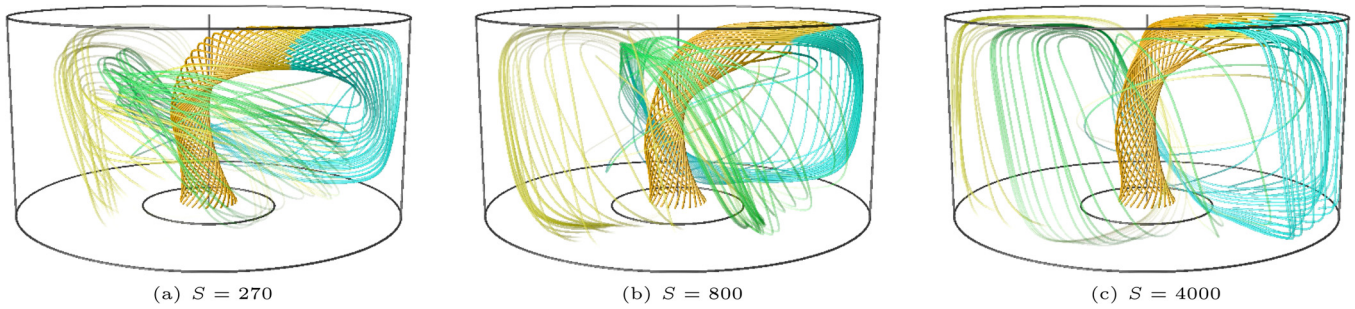

FIG. 9. Field lines entering through the central electrode form a helical column that rotates almost rigidly. The prolongation of the central flux tube is strongly affected by the Lundquist number.

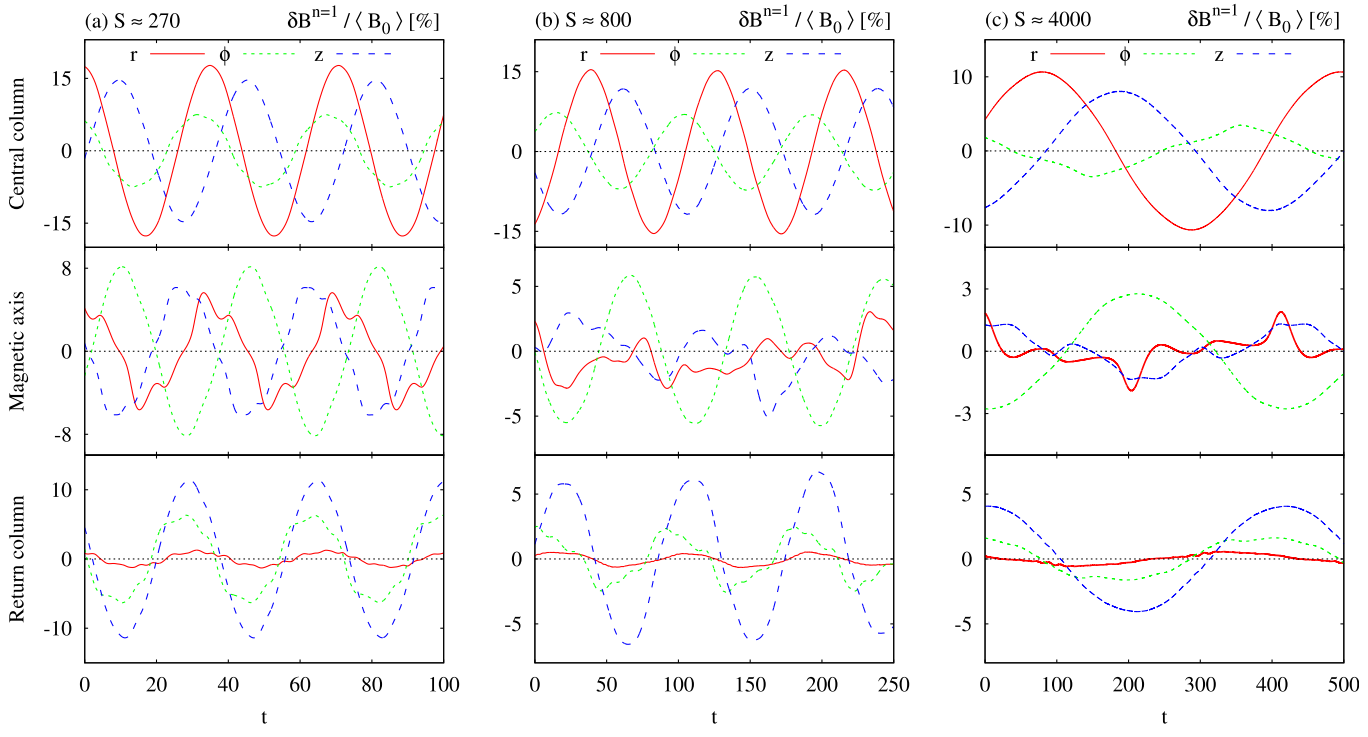

FIG. 10. Evolution of the relative magnetic fluctuations of the $n = 1$ mode in three spatial locations: near the axis of symmetry (central column), at the magnetic axis, and near the wall (return column). All values are taken at $z = 0.5$. The three components of the magnetic field vector are displayed for three cases.

The profiles shown in Fig. 7 are computed with the $n=0$ mode alone. We also want to assess the toroidal structures arising in the different regimes of sustainment. Figure 8 shows colormaps of the instantaneous value of λ, during sustainment, in the toroidal cross section at $z=0.5$. The black lines show the cross section the column of flux coming from the electrode and its return near the wall (see Sec. III C). Note that a high field-aligned current is present there in all cases. Also note that λ is highly non-uniform in the whole toroidal plane for low S values. At high S, λ becomes more uniform in the closed flux region, but still exhibits some spatial structure in the central open flux column. This agrees with measurements in SSPX[18] that indicates that λ is not uniform in the open flux region.

C. Helical distortion of the central column of flux

The observation of coherent oscillations of the $n=1$ mode is ubiquitous in spheromak sustainment experiments.[5,10,12] These oscillations were found to be due to a rotating helical distortion of the open linked flux.[16–18] The formation of this central column and its behavior during sustainment were already reproduced using tangential boundary flows.[6,26] Here, we extend the analysis by considering the effect of the Lundquist number.

Fig. 9 shows the central flux column and its prolongation for three S values. For each case, twenty four lines are followed from $r=0.15$ to $z=0$ at the central electrode. All lines have a normalized distance equal to ten. The central column is shown in orange and the primary return column in cyan. Since several lines of the return column do not cross the outer electrode immediately, their color is switched each time they pass close to the geometrical axis, first to green and then to yellow.

When resistivity is high ($S=270$), the return column is strongly distorted and the field lines of its prolongation wander through a large volume of the plasma. As S increases, the helical distortion of the central column diminishes and the return column as well as its prolongation is pushed towards the flux conserver walls, leaving a larger volume of plasma unaffected. The behavior of the field lines during sustainment is complex and deserves additional studies that are left for future work.

D. Magnetic fluctuations

Fig. 10 shows the evolution of the three components of the magnetic field vector of the $n=1$ mode, at three spatial locations: near the axis of symmetry ($r=0.08$), at the magnetic axis ($r=0.61$), and near the wall ($r=0.92$). All values are taken at $z=0.5$ and are normalized with the local average magnetic field $\langle B_0\rangle$.

In agreement with the presence of the rotating column, the magnetic fluctuations show a sinusoidal evolution near the axis of symmetry and near the wall. At the magnetic axis, only the toroidal component (which is parallel to the mean field there) has a sinusoidal evolution with the same frequency. This is due to the rotating open flux column, since it may regarded as a rotating current loop that induces magnetic flux in its interior. In contrast, the poloidal components of the fluctuation have a different and *a priori* uncorrelated evolution. It is important to keep in mind that these latter components are responsible, along with the poloidal velocity fluctuations, for the dynamo electric field that sustains the configuration (see Sec. III F).

The above discussion suggests that parallel and perpendicular fluctuations should be considered separately. This is done in Fig. 11. The mean fluctuation level, relative to the mean field, at the magnetic axis during sustainment is shown as a function of the Lundquist number, for (a) the parallel and (b) the perpendicular components. While the parallel fluctuation with $n=1$ is clearly dominant, the amplitudes of the perpendicular fluctuations with $n=1$ and $n=2$ are much closer. In fact, the amplitude of the $n=2$ fluctuation is larger than that of the $n=1$ for $220 \lesssim S \lesssim 450$.

It is interesting to analyze the behavior of fluctuations in the high Lundquist regime. On one hand, the perpendicular fluctuations decrease rapidly with S since less dynamo action is required for sustainment. On the other hand, the parallel fluctuations induced by the central column decay more slowly.

The frequency of rotation of the open flux column can be deduced from the frequency of $n=1$ magnetic fluctuation signal either at the axis of symmetry or near the wall (the frequency of the parallel fluctuation at the magnetic axis could be

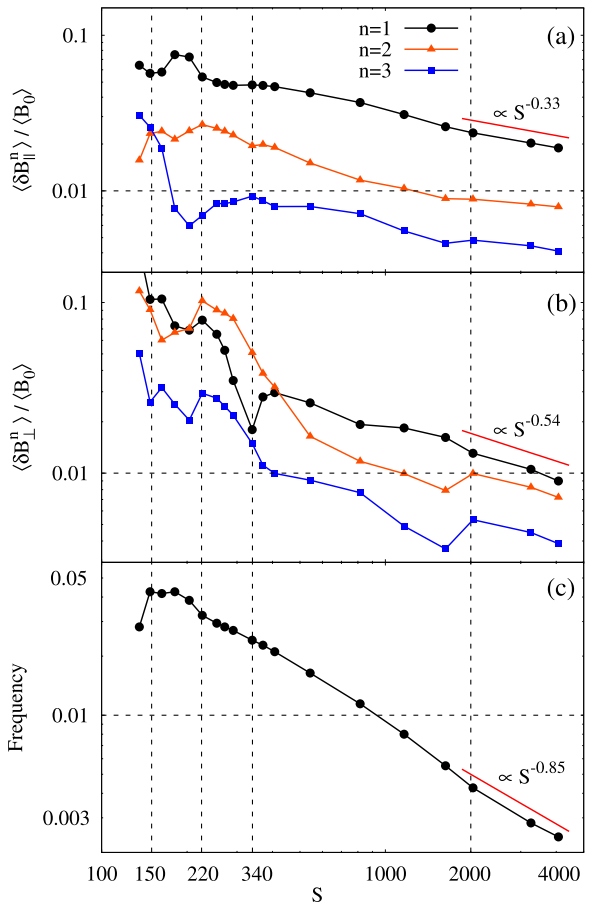

FIG. 11. Mean fluctuation level, relative to the mean field, of the three dominant modes during sustainment at the magnetic axis as a function of S: (a) parallel and (b) perpendicular components. (c) The frequency of the parallel fluctuation, normalized with the Alfvén time, is also shown.

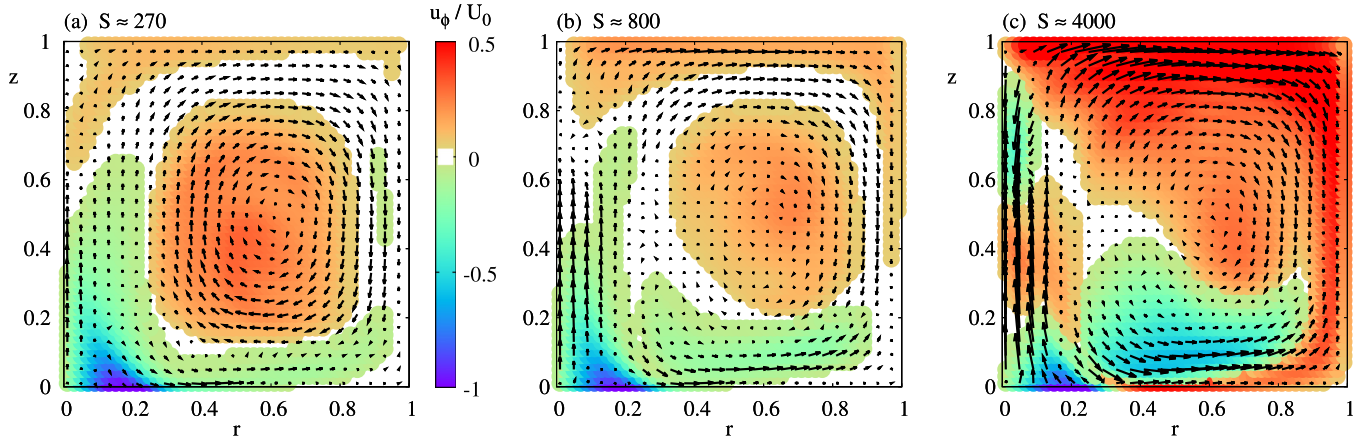

FIG. 12. Mean flow during sustainment. The colormaps indicate the toroidal flow and the arrows indicate the poloidal flow. The flow is normalized with the corresponding U_0 value in each case.

used as well). This frequency is shown, as a function of S, in Fig. 11(c). The behavior resembles a power law that is only slightly affected by the different regimes of sustainment. The frequency is nondimensionalized by multiplying it by the Alfvén time and can be (roughly) compared with values from experiments. Taking data from SPHEX[16] ($a \sim 0.4$ m, $c_A \sim 8 \times 10^5$ m/s, $f \sim 20$ kHz, and $\tau_r \sim 1$ ms) yields $f_{exp} \sim 10^{-2}$ for the dimensionless frequency and $S_{exp} \sim 2000$ for the Lundquist number. This value agrees within an order of magnitude with our results, as can be seen in Fig. 11(c).

E. Velocity profiles

The (almost) rigid rotation of the open flux column does not imply the rotation of the plasma as a whole as pointed out in Ref. 6. This can be observed in Fig. 12, where the mean flow in the poloidal plane during sustainment is shown for three regimes of sustainment. Toroidal and poloidal flows are shown by colormaps and arrows, respectively. Clearly, the mean toroidal flow follows the external driving flow only near the electrode but it reverses its sign at the magnetic axis and near the upper and lateral walls. White regions indicate that the toroidal flow is close to zero.

The previous description was focused on the mean flow and involved only the axisymmetric part of the solution ($n = 0$ mode). The toroidal structure of the flows is shown in Fig. 13. The instantaneous velocity field at $z = 0.5$ is displayed for three Lundquist values. In this case, colormaps indicate the vertical flow and the arrows indicate the toroidal and radial components of the flow. The open flux column (central and return) is shown with yellow lines.

The structure of the flow is complex and not axisymmetric but roughly speaking, the flow points upward in the central region and downward in the periphery (some reversals are observed at high S values, however), approximately aligned with the magnetic field. Although we have observed significant fluctuations in the velocity fields, the flow patterns of Fig. 13 are qualitatively held as they rotate following the open flux column. Note the vortex structures near the central flux tube. They could be related with the rapid vortex like motions about the central helical axis that have been inferred from electric field measurements in SPHEX.[16]

F. MHD dynamo

The correlated fluctuations of velocity ($\tilde{\mathbf{u}}$) and magnetic field ($\tilde{\mathbf{B}}$) induce an electric field with a non-zero component along the mean magnetic field. This electric field acts to redistribute the externally driven current in the magnetic configuration and is commonly referred to as the MHD

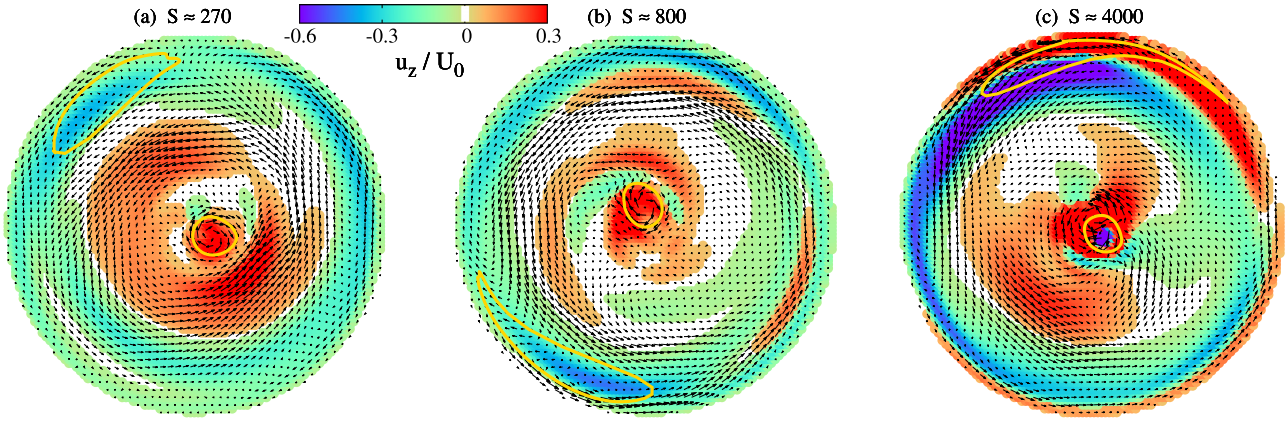

FIG. 13. Instantaneous velocity fields in the toroidal plane (at $z = 0.5$) during sustainment. Vertical flow is indicated by colormaps and toroidal and radial flows by arrows. The central flux column and its primary return are shown with yellow lines.

dynamo. It may be computed as $E_{dyn} = \langle \tilde{\mathbf{u}} \times \tilde{\mathbf{B}} \rangle \cdot \mathbf{b}$, where $\mathbf{b}$ is the unit vector in the mean magnetic field direction and $\langle \cdot \rangle$ typically denotes time averaging.[12] In our setting, however, it is convenient to consider the toroidal modes separately and perform toroidal averaging. This allows us to compute the instantaneous dynamo electric field (which, in turn, can be averaged in time) and distinguish the contribution of each mode. Thus, the total dynamo electric field is expressed as $E_{dyn} = \sum_n E^n_{dyn}$, and its temporal average as $\bar{E}_{dyn}$. Note that only fluctuations of velocity and magnetic field with the same toroidal number contribute to the dynamo electric field.

The first row of Figs. 14(a.1) to 14(c.1) shows colormaps of $\bar{E}_{dyn}$ multiplied by the radial coordinate in the poloidal plane. The quantity $r\bar{E}_{dyn}$ is proportional to the loop voltage required to balance resistive dissipation. In particular, Faraday's law integrated along the magnetic axis yields $(r\bar{E}_{dyn})_{ma} = (r\eta\bar{J}_\phi)_{ma}$ in steady state. For this reason, the values in Fig. 14 are normalized with $(r\eta\bar{J}_\phi)_{ma}$. The black line shows the contour $\bar{E}_{dyn} = 0$, which separates dynamo ($\bar{E}_{dyn} > 0$, i.e., same sense that $\langle B_0 \rangle$) from antidynamo ($\bar{E}_{dyn} < 0$, i.e., opposite sense that $\langle B_0 \rangle$) regions. A complex structure of strong dynamo and antidynamo regions is

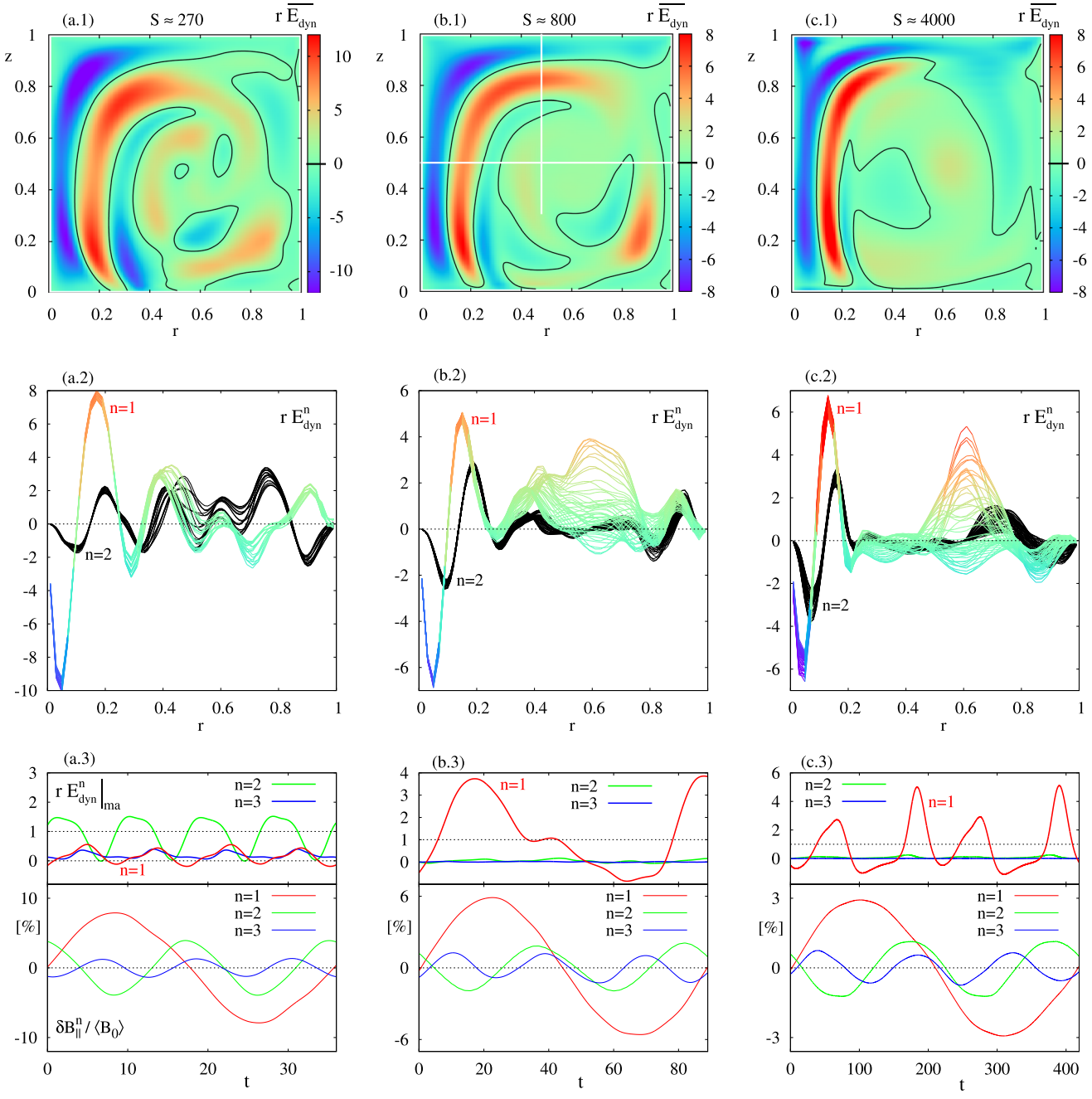

FIG. 14. Colormaps of the mean (in time) total dynamo electric field multiplied by the radial coordinate (a.1)–(c.1). The black line is the contour $r\bar{E}_{dyn} = 0$. Several radial profiles of the instantaneous value of rE^n_{dyn} for $n = 1$ and $n = 2$, at $z = 0.5$ (a.2)–(c.2). The color scale of the $n = 1$ profiles is the same than that of the corresponding colormap. Evolution of rE^n_{dyn} at the magnetic axis and the relative parallel magnetic fluctuation for $n = 1$, 2, and 3 (a.3)–(c.3). All values are normalized with $(r\eta\bar{J}_\theta)_{ma}$.

observed for low Lundquist numbers [Fig. 14(a.1)]. The structure becomes more organized for higher values of S. Note that, for $S = 4000$ [Fig. 14(c.1)], the dynamo region becomes simply connected and has a peak around the magnetic axis.

Several instantaneous radial profiles of rE^n_{dyn} for $n = 1$ and $n = 2$ are shown in Figs. 14(a.2) to 14(a.2). The antidynamo-dynamo structure of the central column is a robust feature present in all regimes of sustainment. The value of the electric field there remains nearly constant in time (it has small amplitude fluctuations). This is a clear indication that the magnetic and velocity fluctuations oscillate in phase (they approximately rotate) in that region (see Fig. 15). By contrast, the dynamo action of each toroidal mode in the closed flux region ($0.2 \lesssim r \lesssim 0.8$ in this plot) has large relative oscillations in time.

The temporal dependence of E^n_{dyn} at the magnetic axis is shown in Figs. 14(a.3) to 14(c.3). The time interval in each case is chosen to match one period of oscillation of the parallel magnetic fluctuation (related to the rotation of the central column), shown in the lower panel. Note that the dynamo action produced by the perpendicular fluctuations has very different behaviors in each regime. Furthermore, each evolution seems *a priori* uncorrelated from the parallel magnetic fluctuation, and thus, uncorrelated from the central column's rotation.

The results presented in this section are in remarkable agreement with the dynamo effect observations in SPHEX.[12] The radial and traverse profiles of E_{dyn} obtained for the $S = 800$ case at the locations indicated with white lines in Fig. 14(b.1) are shown in Figs. 15(a) and 15(b). These results closely resemble the experimental profiles shown in Figs. 4 and 6 of Ref. 12. On the other hand, by studying the temporal behavior of the fluctuations al-Karkhy and co-workers identified two different mechanisms: a single-mode dynamo and a "turbulent" dynamo. The former was located at the central column and was characterized by highly correlated fluctuations associated with the dominant $n = 1$ mode, while the latter was identified at the magnetic axis and produced by poorly correlated fluctuations and a different frequency spectrum (the dynamo did not vanish when the frequency of the $n = 1$ mode and its harmonics were filtered out). The same picture is found here. Consider the time series of the perpendicular (to the local mean field) velocity and magnetic fluctuations of the $n = 1$ mode that are shown in Fig. 15(c). The amplitude of the signal is conveniently rescaled for the ease of comparison. The correlation of the $n = 1$ fluctuations is very high at the geometric axis but very low at the magnetic axis. We recall that this is valid only for the perpendicular fluctuation, since the parallel component is highly correlated with the rotation of the column, as shown in Sec. III D.

Finally, we note that for low Lundquist values, e.g., $S = 270$, the dominant contribution to the dynamo at the magnetic axis comes from the $n = 2$ mode, even though the $n = 1$ mode contains more magnetic energy, as can be seen in Fig. 3(b). This is in agreement with data in Fig. 11, where we saw that the $n = 2$ perpendicular fluctuation is larger than the $n = 1$ perpendicular fluctuation for $200 < S < 400$. Fig. 16 shows the contributions of the first three toroidal modes to the average dynamo electric field at the magnetic axis as a function of S. The $n = 1$ dominates the current redistribution process for $S > 400$. Note, however, that there is an observable trend of the $n = 2$ contribution to grow for $S \gtrsim 2000$. This may indicate the existence of interesting phenomena at higher Lundquist values. Unfortunately, to perform a confident exploration of such high S regime in a reasonable computation time, improvements in the present capabilities are needed, either by improving the code's performance, computing power or both.

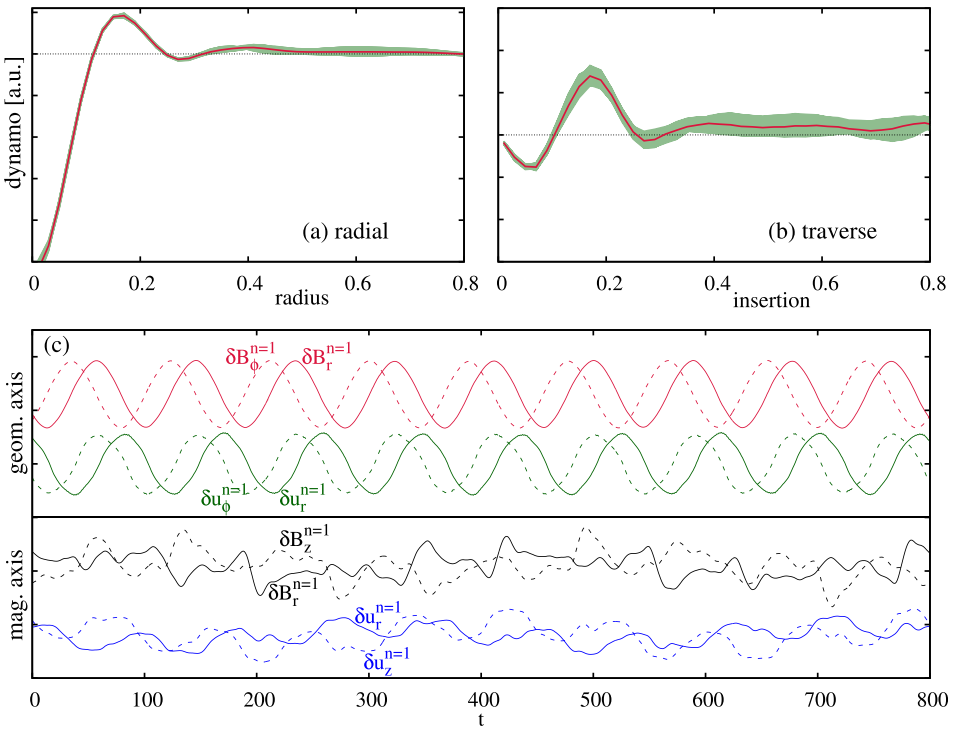

FIG. 15. (a) Radial and (b) traverse E_{dyn} profiles obtained at the locations indicated with white lines in Fig. 14(b.1). (c) Temporal signals of the perpendicular $n = 1$ fluctuations of velocity and magnetic field at the geometric and magnetic axis.

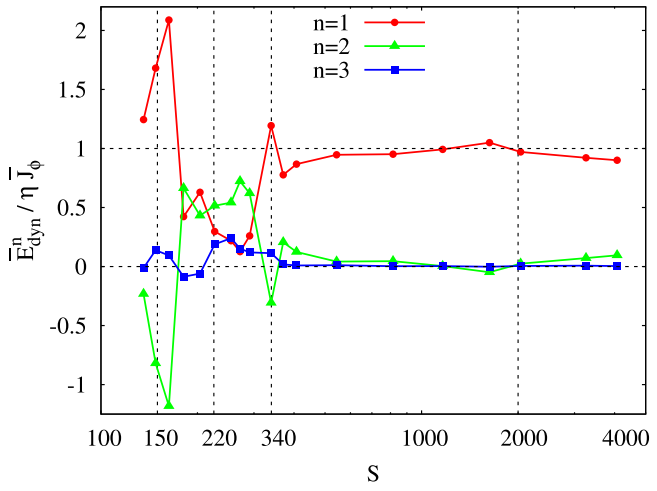

FIG. 16. Average dynamo electric field at the magnetic axis of the first three toroidal modes.

IV. CONCLUSIONS

Several aspects of the dynamics of the MHD activity during spheromak sustainment have been addressed using nonlinear numerical simulations. The initial condition was chosen to model the magnetic configuration observed in spheromak experiments driven by coaxial plasma guns. Tangential boundary flows were used to inject magnetic helicity at different rates. By changing the Lundquist number adequately, the balance between helicity injection and dissipation was achieved for mean magnetic configurations very similar to the initial condition (for $S > 150$). In this way, different regimes of operation were accessed and studied. The main findings are summarized below.

The mean magnetic configuration during sustainment was very similar to the initial condition for a large range of Lundquist numbers. Although small deviation in the total magnetic energy and helicity contents were observed, the relaxation behavior (in terms of minimization of magnetic energy relative to helicity) was satisfied with remarkable accuracy. This was true for $S > 150$. For smaller Lundquist numbers, the relaxation process was not able to sustain the configuration close to the initial condition.

In agreement with the existing experimental evidence, the $\lambda(\psi)$ profile during sustainment remained close to a linear profile with normalized slope $\alpha = -0.4$. However, different regimes of operation were identified. The high Lundquist regime ($S > 2000$, most relevant to experiments) was characterized by a region with a flat q approximately equal to one around the magnetic axis and small oscillations in q_a. As the helicity injection rate was increased (and S decreased), the amplitude of the oscillations grew significantly as well as the mean value of q_a. At $S \approx 350$, a transition was observed in which q_a reached a maximum and the oscillations disappeared. This low S regime was characterized by a high magnetic shear in the magnetic axis region and a different behavior of the modes. In particular, the $n = 2$ became dominant in the production of the dynamo action along the magnetic axis. Since this regime was observed at low Lundquist values, it may be considered of little practical relevance. However, it is interesting from a theoretical point of view since it shows that the relaxation behavior (minimization of magnetic energy relative to helicity) can be effectively achieved with different mean profiles of the safety factor and different dynamics of the modes. On the other hand, the results presented here suggest that the presence of a resonant $q = 1$ magnetic surface is a fundamental feature required for magnetic relaxation in spheromaks.

The helical distortion and rotation of the central flux column, which is an ubiquitous feature in spheromak sustainment (and other devices such as coaxial plasma thrusters), was recovered and studied. As expected, for increasing Lundquist numbers (and decreasing helicity injection rate), the distortion of the column as well as the rotation frequency decreased. We have shown that this phenomenon does not imply the rotation of the plasma as a whole. Instead, it is produced by the coherent oscillation of the $n = 1$ mode, including both velocity and magnetic fluctuations, in the central region and near the wall of the flux conserver. Moreover, our simulations indicate that this mode does not rotate rigidly either. At the magnetic axis, only the parallel magnetic fluctuation (toroidal component) is coherent with the column's rotation. The perpendicular components, by contrast, show an uncorrelated evolution. These results are in remarkable agreement with measurements of the dynamo in SPHEX,[12] and thus, they provide compelling evidence indicating that the dynamics of magnetic relaxation in spheromaks is well described by the MHD model.

Despite the high level of agreement with pre-existing experimental data, there are some aspects that could not be recovered using the present numerical model. In particular, we were not able to reproduce the feedback mechanism reported in Refs. 5 and 16 that limit the maximum flux amplification attainable. It was observed that ψ_a/ψ_G remained approximately fixed at $\sim$5 for a broad range of gun parameters.[5] Furthermore, when the power required for sustainment was reduced (by using titanium gettering), the reduction in the power transfer was achieved not by a decrease in the saturation amplitude of the mode but by switching the mode off and back on to a fixed amplitude.[16] We observed neither a limit in ψ_a/ψ_G (in typical, physically relevant, conditions) nor an episodic stabilization of the mode. Instead, we observed a continuous reduction of the modes amplitudes. This may be a crucial issue for a deeper understanding of the operation of coaxial plasma guns and deserves additional efforts. One possible source for this discrepancy may be the neglect of flux leakage through the non-electrode walls. As pointed out by Holcomb *et al.*,[18] the common assumption that the 100% of ψ_G remains connected to the electrodes during sustainment is generally (probably always) false. The addition of a model of flux leakage will be considered in future works.

Finally, we mention that a careful election of the tangential boundary flow profile could lead to a better approximation of the actual electric field imposed by the gun in spheromak experiments and, thus, an improved and possibly quantitative model could be obtained. More, in general, this paper shows that tangential boundary flows can be used to

model the effect of electric fields in helicity injected devices within the framework of the MHD model.

[1]T. R. Jarboe, Plasma Phys. Controlled Fusion **36**, 945 (1994).
[2]J. B. Taylor, Phys. Rev. Lett. **33**, 1139 (1974).
[3]T. R. Jarboe, I. Henins, A. R. Sherwood, C. W. Barnes, and H. W. Hoida, Phys. Rev. Lett. **51**, 39 (1983).
[4]C. W. Barnes, J. C. Fernández, I. Henins, H. W. Hoida, T. R. Jarboe, S. O. Knox, G. J. Marklin, and K. F. McKenna, Phys. Fluids **29**, 3415 (1986).
[5]M. G. Rusbridge, S. J. Gee, P. K. Browning, G. Cunningham, R. C. Duck, A. al-Karkhy, R. Martin, and J. W. Bradley, Plasma Phys. Controlled Fusion **39**, 683 (1997).
[6]P. L. García Martínez and R. Farengo, Phys. Plasmas **17**, 050701 (2010).
[7]M. A. Berger and G. B. Field, J. Fluid Mech. **147**, 133 (1984).
[8]J. Heyvaerts and E. R. Priest, Astron. Astrophys. **137**, 63 (1984).
[9]T. G. Cowling, Mon. Not. R. Astron. Soc. **94**, 768 (1934).
[10]S. O. Knox, C. W. Barnes, G. J. Marklin, T. R. Jarboe, I. Henins, H. W. Hoida, and B. L. Wright, Phys. Rev. Lett. **56**, 842 (1986).
[11]E. B. Hooper, L. D. Pearlstein, and R. H. Bulmer, Nucl. Fusion **39**, 863 (1999).
[12]A. al-Karkhy, P. K. Browning, G. Cunningham, S. J. Gee, and M. G. Rusbridge, Phys. Rev. Lett. **70**, 1814 (1993).
[13]C. R. Sovinec, J. M. Finn, and D. Del-Castillo-Negrete, Phys. Plasmas **8**, 475 (2001).
[14]B. I. Cohen, E. B. Hooper, R. H. Cohen, D. Hill, H. S. McLean, R. D. Wood, S. Woodruff, C. R. Sovinec, and G. A. Cone, Phys. Plasmas **12**, 056106 (2005).
[15]B. I. Cohen, C. A. Romero-Talamás, D. D. Ryutov, E. B. Hooper, L. L. Lodestro, H. S. McLean, T. L. Stewart, and R. D. Wood, Phys. Plasmas **16**, 042501 (2009).
[16]R. C. Duck, P. K. Browning, G. Cunningham, S. J. Gee, A. al-Karkhy, R. Martin, and M. G. Rusbridge, Plasma Phys. Controlled Fusion **39**, 715 (1997).
[17]S. Woodruff and M. Nagata, Plasma Phys. Controlled Fusion **44**, 2539 (2002).
[18]C. T. Holcomb, T. R. Jarboe, D. N. Hill, S. Woodruff, and R. D. Wood, Phys. Plasmas **13**, 022504 (2006).
[19]D. M. Willett, P. K. Browning, S. Woodruff, and K. J. Gibson, Plasma Phys. Controlled Fusion **41**, 595 (1999).
[20]R. J. Leveque, *Finite Volume Methods for Hyperbolic Problems* (Cambridge University Press, Cambridge, 2002).
[21]G. Toth, Astrophys. Lett. Commun. **34**, 245 (1996).
[22]G. Toth, J. Comput. Phys. **161**, 605 (2000).
[23]P. L. Roe and D. S. Balsara, SIAM J. Appl. Math. **56**, 57 (1996).
[24]D. S. Balsara, Astrophys. J. Suppl. **116**, 119 (1998).
[25]P. L. García Martínez and R. Farengo, Phys. Plasmas **16**, 082507 (2009).
[26]P. L. García Martínez and R. Farengo, Phys. Plasmas **16**, 112508 (2009).
[27]V. A. Izzo and T. R. Jarboe, Phys. Plasmas **10**, 2903 (2003).
[28]J. B. Taylor, Rev. Mod. Phys. **58**, 741 (1986).
[29]D. P. Brennan, P. K. Browning, and R. A. M. van der Linden, Phys. Plasmas **9**, 3526 (2002).
[30]J. M. Finn and T. M. Antonsen, Comments Plasma Phys. Controlled Fusion **9**(3), 111–126 (1985).
[31]M. A. Berger, in *Magnetic Helicity in Space and Laboratory Plasmas*, edited by M. R. Brown, R. C. Canfield, and A. A. Pevtsov (American Geophysical Union, Washington, DC, 1999), p. 1.
[32]K. Galsgaard and Å. Nordlund, J. Geophys. Res. **101**, 13445, doi:10.1029/96JA00428 (1996).